Journal of The Electrochemical Society

Transition Metal Oxides as DMFC Cathodes Without Platinum

Journal of The Electrochemical Society, **154** (7) B664-B669 (2007)
0013-4651/2007/154(7)/B664/6/$20.00 © The Electrochemical Society

Transition Metal Oxides as DMFC Cathodes Without Platinum

Yan Liu,[a,b,z] Akimitsu Ishihara,[a] Shigenori Mitsushima,[a,b,*] Nobuyuki Kamiya,[a,*] and Ken-ichiro Ota[a,*]

[a]*Chemical Energy Laboratory, Yokohama National University, Hodogaya-ku, Yokohama 240-8501, Japan*
[b]*State Key Laboratory for Structural Chemistry of Unstable and Stable Species, Institute of Physical Chemistry, College of Chemistry and Molecular Engineering, Peking University, Beijing 100871, China*

Transition metal oxides (ZrO_2, TiO_2, SnO_2, Nb_2O_5, and Co_3O_4) made by sputtering methods were investigated as new electrocatalysts for the cathode of a direct methanol fuel cell (DMFC) without platinum. The catalytic activity for the oxygen reduction of these transition metal oxides was evaluated in sulfuric acid with and without 0.1 M methanol. The sputtered metal oxides had stable states in acid medium at least in the potential range of the oxygen reduction. The metal oxides were not active for the methanol oxidation. The oxygen reduction activity of the metal oxides decreased in the following order: $ZrO_{2-x} > Co_3O_{4-x} > TiO_{2-x} \approx SnO_{2-x} > Nb_2O_{5-x}$ in the presence of methanol. Zirconium oxides showed the best activity for the oxygen reduction among these transition metal oxides. Moreover, in comparison with the sputtered Pt, the potential at $i_{O_2-N_2} = -5\ \mu A\ cm^{-2}$ of ZrO_{2-x} was 60 mV larger than that of the sputtered Pt. This is due to the high selectivity of the metal oxides for the oxygen reduction. The mixed potential as found on the Pt electrode was not observed on the metal oxide catalysts. Zirconium oxides could be a good cathode substituting the platinum cathode for DMFCs.
 [DOI: 10.1149/1.2734880]

Manuscript submitted April 28, 2006; revised manuscript received February 27, 2007. Available electronically May 16, 2007.

Much attention has been paid to direct methanol fuel cells (DMFCs) because a direct-fed liquid fuel cell is ideal for portable power and mobile applications due to its compact system and high energy density for fuel storage. However, the commercial success of DMFCs has not yet been realized, mainly because of its low fuel efficiency and power density. The major energy losses are caused by the poor activity of methanol oxidation and methanol crossover[1,2] from the anode to the cathode through the commonly used sulfonated perfluoronated membrane, such as Nafion. Highly dispersed platinum on carbon powder has been widely used as an oxygen reduction electrocatalyst in DMFC systems. Most Pt-based cathode materials are also catalytically reactive to the methanol oxidation reaction (MOR). Performance losses caused by methanol crossover arise from the fact that a mixed cathode potential is established which is far more negative when comparing the cathode potential in the absence of methanol. Platinum is expensive and resources are very limited. Considering the cost and resource of platinum, many attempts are on-going to reduce the Pt loading. However, there appears a new problem: Pt dissolution and deposition in the electrolyte.[3-5] These will be a limit of the reduction of the Pt loading. Therefore, the development of stable, methanol-tolerant, and nonplatinum catalysts for the oxygen reduction is very important for a wide application of DMFCs.

Many efforts have been made to develop methanol-tolerant nonplatinum catalysts for the oxygen reduction. They were mostly metal complexes. These include: macrocycles, such as the CoTAA (cobalt tetrazaanelene) electrodeposited on graphite power embedded in a cast Nafion film,[6] Fe–tetranitrophenylporphyrine [Fe-PP$(NO_2)_4$],[7,8] the heat-treated CoTPP/FcTPP (tetraphenylporphyrine) mixture,[9] and the heat-treated binary metalloporphyrine, which was found to have higher activity for the ORR compared to a single-metal heat-treated metalloporphyrin.[10] The heat-treated μ–oxo–iron (III) tetramethoxy phenyl porphyrine (Fe–TMPP)$_2$, iron (III) tetramethoxy phenyl porphyrine (Fe–TMPP–Cl) and iron (III) octaethyl porphyrine (FeOEP–Cl) adsorbed on high-area carbons in the electrolyte of 85% H_3PO_4 equilibrated Nafion 117 membrane at 125°C and hydrated Nafion membrane at 60°C[11,12] have been also reported as the methanol-tolerant oxygen reduction catalysts. Some of these materials have been reported to be nonreactive to the methanol oxidation and to show a comparable performance of Pt for the oxidation reduction. However, long-term stability against chemical/electrochemical attack is a barrier for application of these macrocyclic complexes.[13] Transition metal sulfides which have Chevrel phases (M_6X_8, M = high valent transition metal, X = chalcogen), such as Ru_xSe_y were reported to be highly selective toward the oxygen reduction in the presence of methanol.[14] Among the mixed cluster compound $Mo_{6-x}M_xX_8$ (M = Ru, Os, Rh, and Pt;[15] X = S,[16,17] Te,[15-17] Se,[18,19]), the compounds that have Mo and Ru are relatively active for the oxygen reduction. $Mo_4Ru_2Se_8$ immersed in oxygen-saturated sulfuric acid, performed with similar characteristics of Pt in the absence of methanol, and inactive to methanol.[20] Long-term chemical stability is probably a more serious issue for these catalysts, as for the porphyrin-based materials.[13]

We have reported that zirconium oxide (ZrO_{2-x}) has a clear activity for the oxygen reduction and is stable in acid medium.[21] The equilibrium concentration of zirconium ion (saturated solubility) of zirconium oxide is 3×10^{-7} M in 1 M H_2SO_4 at 70°C.[21] On the other hand, the equilibrium concentration of Pt^{2+} for the Pt/C is 1×10^{-6} M in 0.5 M H_2SO_4, 80°C at 1.0 V vs RHE.[5] Zirconium oxide might have a higher chemical stability in an acidic media than that of the Pt/C, because the solubility of zirconium is smaller than that of Pt. In this study, transition metal oxides were investigated as new electrocatalysts for the cathode of DMFC, where the catalysts should be active for the oxygen reduction and inactive for the methanol oxidation. The electrochemical behavior of transition metal oxide catalysts made by sputtering methods was evaluated for the oxygen reduction in sulfuric acid with and without methanol.

Experimental

The transition metal oxide catalysts were sputtered on the end of a glassy carbon rod substrate (5.2 Ø × 10 mm length, Tokai Carbon) by a radio-frequency (rf) magnetron sputtering method using an MUE-ECO-EV apparatus (ULVAC). Prior to the sputtering, the surface of the glassy carbon was polished by lapping tape LT-2000, LT-4000, and LT-6000 (Fuji Film Co., Japan) by turns to a mirror finish. The metal oxide target (ZrO_2, TiO_2, SnO_2, Nb_2O_5, Co_3O_4, 99.9% purity, Furuuchi Chemical Co., Japan), with a diameter of 50.7 mm, was fixed on a cooled cathode. Before deposition, the vacuum chamber was evacuated down to 10^{-3} Pa using a turbomolecular pump. The sputtering gas, argon with a purity of 99.99% was controlled by a standard mass-flow controller. The sputtering pressure was 3.0×10^{-1} Pa. Before deposition, the target was cleaned by sputtering with an rf power of 50 W for 5 min, while the glassy carbon was covered with a shield. The rf power was changed from 80 to 150 W to get a deposition rate of 0.3 Å s^{-1} for each target. The glassy carbon rod was heated at 500°C by a halogen lamp heater during the sputtering. A Pt electrode deposited at unheated condition was also fabricated for comparison. The distance between

* Electrochemical Society Active Member.
z E-mail: liu-yan@pku.edu.cn

the target and the glassy carbon was ca. 24 cm. The film thickness was ca. 25 nm measured by a QCM film thickness meter.

The surface and particle morphology were analyzed by field-emission scanning lectron microscope (FE-SEM, JSM-7700F, JEOL, Japan) under an accelerating voltage of 5 kV. The crystalline property of the cross-sectional surface of the metal oxide was observed by transmission electron microscope (TEM, Hitachi H-9500) under an accelerating voltage of 300 kV. The sample of the thicknesses about 60 nm was prepared by focused ion beam (FIB) techniques. The electron diffraction patterns of crystal obtained by fast fourier transform (FFT) of the TEM images were used to determine the crystalline structure.

The crystalline properties for the deposited catalysts on silica plates instead of a glassy carbon were characterized by using the X-ray diffraction (XRD, RINT 2500, Rigaku). The films thickness was ca. 0.5 μm. Data were collected with a scanning speed of $2°\text{min}^{-1}$ over the angular range 10–90° using Cu $K_{\bar{\alpha}}$ (50 kV, 300 mA) radiation in steps of 0.02°.

The electrochemical experiments were conducted in a three-electrode glass cell to do the following electrochemical measurements. (*i*) The electrochemical stability and the MOR activity of the metal oxides were investigated by cyclic voltammetry (CV) in the potential range of 1.2–0.05 V with a scan rate of 50 or 5 mV s^{-1}. (*ii*) After the electrode reached a steady state, the oxygen reduction activity was measured by slow scan voltammetry (SSV) from 1.2 to 0.05 V (cathodic potential scan) with a scan rate of 5 mV s^{-1}. The electrolyte was a 0.1 M (M = mol dm^{-3}) sulfuric acid with or without 0.1 M methanol under an oxygen or a nitrogen atmosphere at 30°C. The reference electrode was a reversible hydrogen electrode (RHE). All the potentials reported in the paper were expressed with respect to a RHE. The catalytic activity for the oxygen reduction reaction (ORR) of all the catalysts was evaluated by the potential-current curve that was obtained from the difference of current density between the O_2 and N_2 atmospheres ($i_{O_2-N_2} = i_{O_2} - i_{N_2}$) in the cathodic potential scan. The current densities were expressed in terms of the geometric surface area of the electrodes. The HZ3000 electrochemical measurement system (Hokuto Denko, Japan) was used in these measurements.

Results and Discussion

SEM and TEM analysis.— The surface morphology of the oxide films deposited at 500°C was analyzed by FE-SEM. The SEM image of zirconium oxide shown in Fig. 1 revealed that the film surface had a highly distributed and homogenous microstructure and the substrate was almost entirely covered by small particles, with an average particle size of ca. 15 nm.

Figures 2a and b show the high-resolution cross-sectional TEM images of zirconium oxide. The electron diffraction patterns obtained by the FFT from the selected area in the TEM image are shown in Fig. 2c and d, respectively. As shown in the TEM images, uniform crystal lattice fringes were observed in most of the particles. The electron diffraction pattern in Fig. 2c shows well-defined (101) lattice fringes with 2.62, 3.2, and 3.2 Å spacing, indicating that the film consists of monoclinic crystalline structure. On the other hand, in Fig. 2d, the lattice fringes with 2.99, 2.99, and 2.58 Å spacing assigned to (111) of hexagonal crystalline structure can be observed. This provides proof that the film deposited at 500°C has high crystallinity and consist of dense, uniform, and randomly oriented nanocrystals (ca. 15 nm). TEM observation also revealed that the thickness of the sputtered film was ca. 25 nm, in good accordance with that measured by a QCM film thickness meter.

XRD analysis.— Figures 3a-e show the XRD patterns of ZrO_{2-x}, SnO_{2-x}, TiO_{2-x}, Co_3O_{4-x}, and Nb_2O_{5-x} films sputtered on a silica plate instead of a glassy carbon with the film thickness of ca. 0.5 μm. In accordance with the TEM results, the characteristic peaks of the monoclinic and hexagonal phase were observed in the ZrO_{2-x} film. The diffraction peaks of the monoclinic phase were predominant and the peaks of the hexagonal phase were relatively weak. A mixture of metal oxides was found in the other oxide films. The cassiterite tin oxide and SnO were observed in the SnO_{2-x} film. Rutile and brookite TiO_2 and Ti_3O_5 were observed in the TiO_{2-x} film, Nb_2O_5 and NbO_2 were observed in the Nb_2O_{5-x} film, and the Co_3O_{4-x} film consisted of CoO and Co_3O_4. Moreover, the sharp diffraction peaks and thin full-width at half-maximum (fwhm) observed in the XRD patterns also indicated that all the metal oxide films deposited at 500°C would have a high crystallinity.

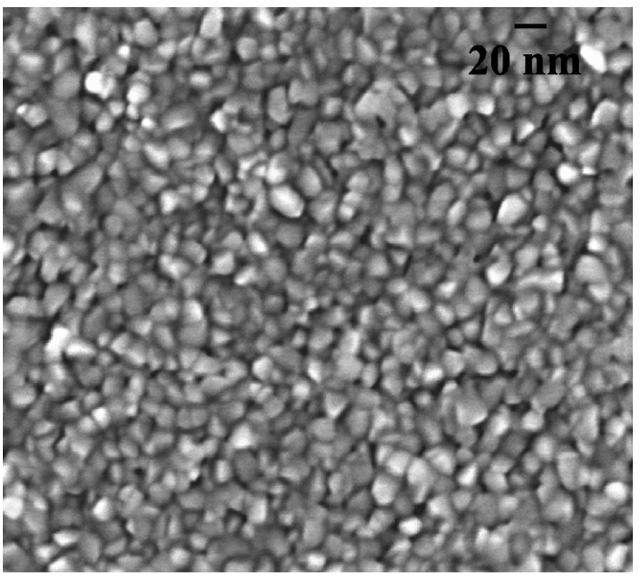

Figure 1. FE-SEM image of zirconium oxide.

Electrochemical stability of metal oxides in acid electrolyte.— Figure 4 shows the cyclic voltammograms (CVs) of the sputtered

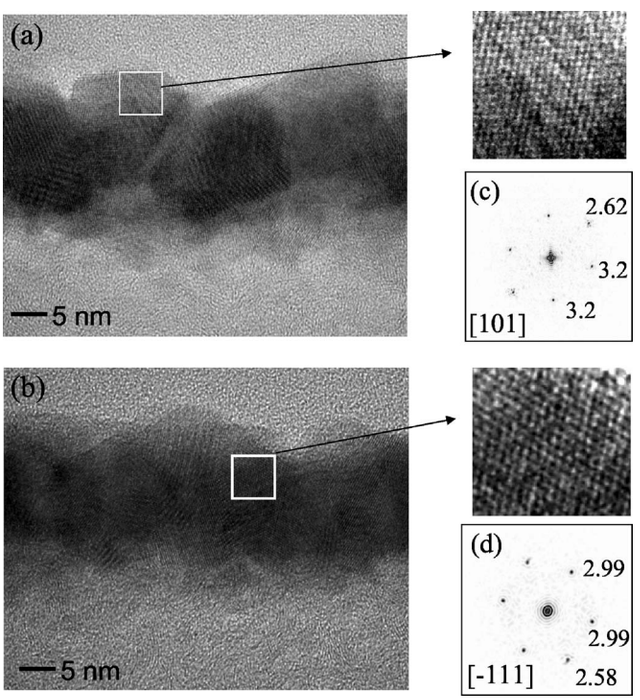

Figure 2. Cross-sectional TEM images and electron diffraction patterns of ZrO_{2-x}.

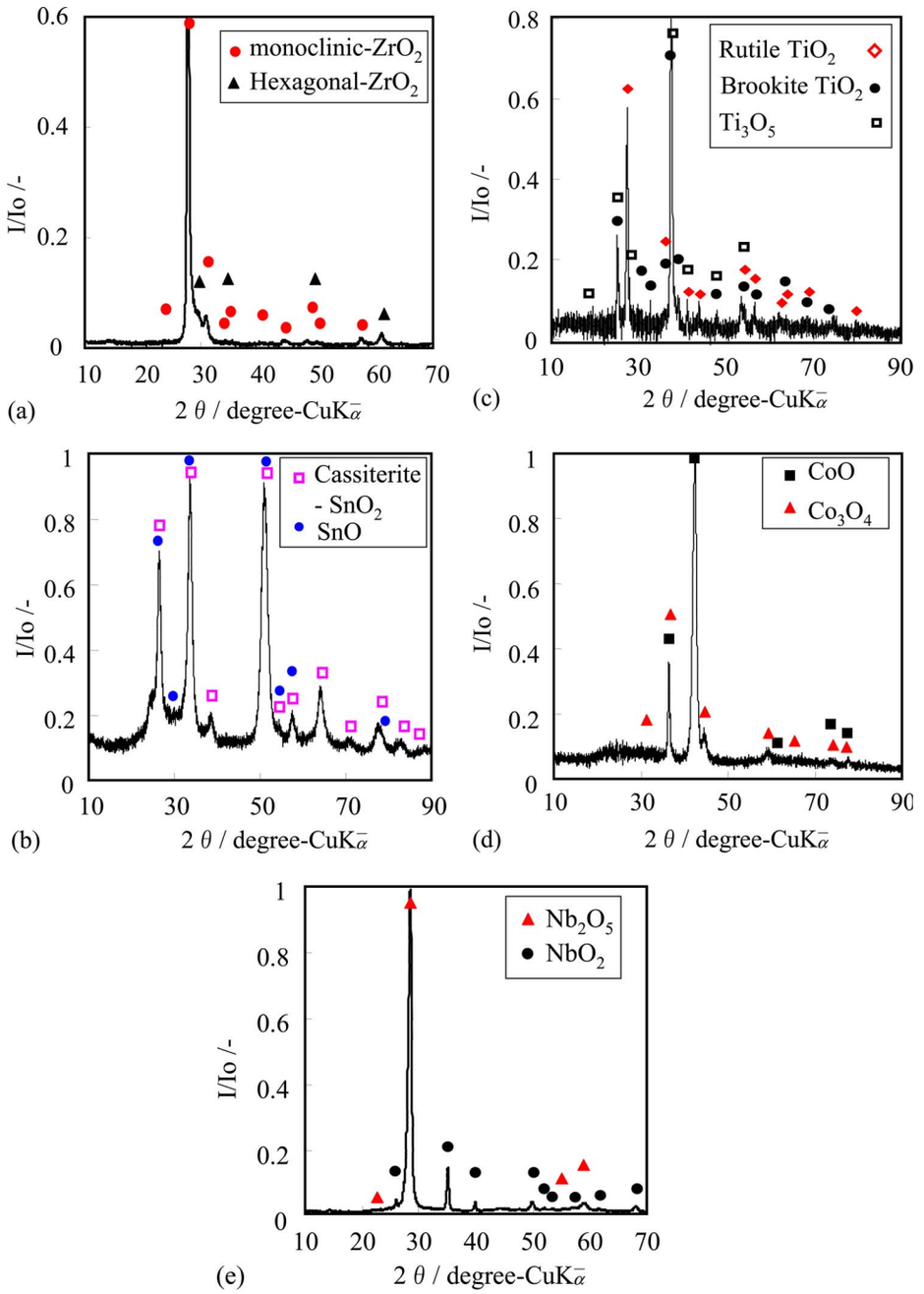

Figure 3. (Color online) XRD patterns of metal oxide film (ca. 0.5 μm) sputtered on a silica plate. (a) ZrO_{2-x}, (b) SnO_{2-x}, (c) TiO_{2-x}, (d) Co_3O_{4-x}, and (e) Nb_2O_{5-x}.

metal oxides in 0.1 M sulfuric acid under a nitrogen atmosphere at 30°C. The potential range was from 1.2 to 0.05 V with a scan rate of 50 mV s^{-1}. No specific oxidation or reduction current peaks were observed in the CVs except for the sputtered Co_3O_{4-x} and the CVs approached a steady state easily after two cycles. For the sputtered Co_3O_{4-x} sample, a reduction current was observed near 1.0 V in the first three cycles. The reduction peaks at E = 1.0 V was considered to be the reaction: $Co_3O_4 + 2H^+ + 2e^- + 2H_2O = 3Co(OH)_2$.[22] However, the CV of the Co_3O_{4-x} also reached a steady state after four cycles. In addition, the oxidation and reduction charges at a steady state presented in the diagonal line were calculated and summarized in Table I. The oxidation charge was close to the reduction charge for all the samples. It indicated quantitatively that a one-sided redox reaction did not occur on these metal oxides. It was considered that the sputtered metal oxides had stable states in acid medium at least in the potential range from 0.7 to 0.9 V for the oxygen reduction.

Catalytic activity of Pt for MOR and ORR.— As a reference for new cathodes, the CVs of the sputtered Pt (s–Pt, 30 nm) and the poly crystalline Pt (Pt wire, poly–Pt) electrodes were investigated in 0.1 M H_2SO_4 under a nitrogen atmosphere with a scan rate of 50 mV s^{-1}. As shown in Fig. 5, the s–Pt showed a similar CV shape in sulfuric acid to that of the poly–Pt, and there was no obvious difference in the current densities and oxidation/reduction peaks between the two types of Pt. Accordingly, the s–Pt could have similar characteristics to the poly–Pt in the sulfuric acid without methanol. The CV of the s–Pt electrode in 0.1 M H_2SO_4 with 0.1 M methanol

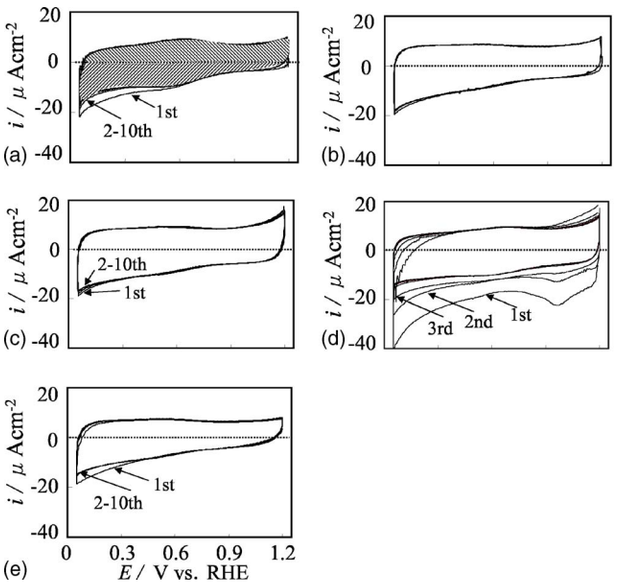

Figure 4. CVs of metal oxides under N_2 atmosphere in 0.1 M H_2SO_4 with 0.1 M methanol at 30°C. Scan rate: 50 mV s^{-1}. (a) ZrO_{2-x}, (b) SnO_{2-x}, (c) TiO_{2-x}, (d) Co_3O_{4-x}, and (e) Nb_2O_{5-x}.

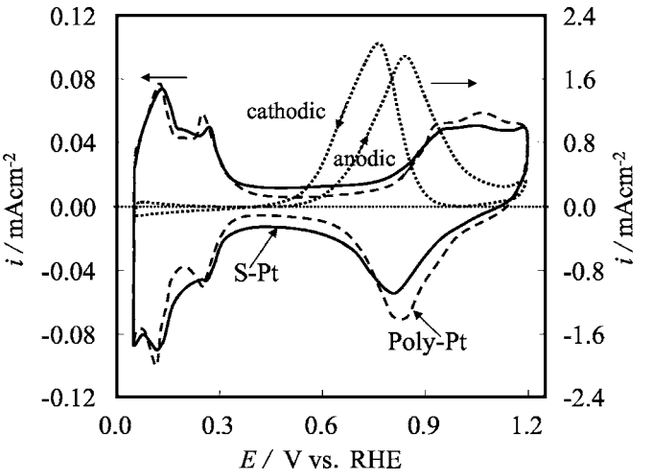

Figure 5. CVs of the s-Pt (30 nm) and poly-Pt under N_2 atmosphere in 0.1 M H_2SO_4. Scan rate: 50 mV s^{-1}. s-Pt without methanol (—), s-Pt with methanol (···), poly-Pt without methanol (---).

under a nitrogen atmosphere is also shown in Fig. 5, which may show the characteristics of the MOR. A large anodic current responded for the methanol oxidation was observed between 0.5 and 1.0 V on the s–Pt electrode. The same trend was observed for the poly–Pt. It is well known that a Pt electrode is catalytically active to the methanol oxidation. A Pt electrode is used for the anode of DMFCs where methanol should be oxidized effectively.

Figure 6 shows the SSV curves of the s–Pt in 0.1 M H_2SO_4 with or without 0.1 M methanol under an oxygen atmosphere. The potential was scanned from 1.2 to 0.05 V (cathodic potential scan) with a scan rate of 5 mV s^{-1}. The oxygen reduction current in methanol free electrolyte shows the well-known behavior: the ORR between 0.65 and 0.95 V proceeds under mixed kinetics of charge transfer and diffusion. The diffusion limited currents are reached below 0.6 V. On the other hand, the current-potential curves under the O_2 atmosphere in the presence of 0.1 M methanol showed an oxidation peak at ca. 0.75 V, where the maximum MOR activity was observed as shown in Fig. 5. The onset potential with respect to the reduction current in the presence of methanol was shifted negatively by about 0.4 V comparing to that in the absence of methanol. This negative shift corresponds to the potential loss of DMFCs due to the methanol crossover to the cathode, although the shift value depends on the methanol concentration.[23,24] Both the MOR and the ORR occurred on the Pt cathode, and led to a mixed cathode potential. In addition, the adsorption of organic species through the methanol oxidation was considered to interfere with the oxygen reduction by blockage of the initial formation of oxygen-containing surface intermediates and/or by interfering with the final conversion of the latter to water.[25]

Catalytic activity of metal oxides for MOR and ORR.— Figure 7 shows the CVs of the sputtered metal oxides in 0.1 M sulfuric acid with or without 0.1 M methanol under a nitrogen atmosphere. The scan rate is 5 mV s^{-1}. It was found that the CVs of the sputtered metal oxides in the presence of methanol were similar to that in the absence of methanol. No clear electro-oxidation current related to the MOR was observed on all the metal oxides. This reveals that these metal oxides were not active for the methanol elctro-oxidation.

Figure 8 shows the SSV curves of the glassy carbon (GC) and the sputtered ZrO_{2-x} electrodes in 0.1 M sulfuric acid with 0.1 M methanol under nitrogen and oxygen atmosphere, respectively. The potential was scanned from 1.2 to 0.05 V with a scan rate of 5 mV s^{-1}. Because the current difference between the nitrogen and oxygen atmosphere appears below 0.4 V on the GC electrode, the reduction of oxygen on the GC took place only below 0.4 V. On the other hand, an apparent increase of reduction current was observed below ca. 0.8 V on the ZrO_{2-x} electrode under the oxygen atmosphere. The current difference between the nitrogen and oxygen atmospheres on the ZrO_{2-x} electrode is assigned to the electroreduction of oxygen. Namely, ZrO_{2-x} has a clear catalytic activity for the oxygen reduction, even in the presence of methanol.

Figure 9 summarizes the potential-current curves obtained from the current difference between oxygen and nitrogen atmospheres ($i_{O_2-N_2} = i_{O_2} - i_{N_2}$) in the cathodic potential scan for all the sputtered metal oxides and the GC. The same as the ZrO_{2-x} electrode, an apparent increase of reduction current was observed for all the other metal oxides samples under the O_2 atmosphere. The potential at the reduction current of -5 μA cm^{-2} [$E_{M-O}(-5)$] was used as the evaluation indicator for the ORR activity in the presence of methanol. The electrode with a larger $E_{M-O}(-5)$ is superior as a DMFC cathode. $E_{M-O}(-5)$ of the Nb_2O_{5-x}, SnO_{2-x}, TiO_{2-x}, Co_3O_{4-x}, and ZrO_{2-x} was 0.22, 0.32, 0.32, 0.43, and 0.68 V, respectively. Therefore, the oxygen reduction activity of the metal oxides would be the following order: $ZrO_{2-x} > Co_3O_{4-x} > TiO_{2-x} \approx SnO_{2-x} > Nb_2O_{5-x}$. ZrO_{2-x} showed the best activity for the oxygen reduction in the presence of 0.1 M methanol among these metal oxides.

Figures 10a and b show the SSV curves of the sputtered metal oxides and the s–Pt electrodes in 0.1 M sulfuric acid with or without 0.1 M methanol under an oxygen atmosphere. The potential

Table I. Oxidation and reduction charge of metal oxides in 0.1 M H_2SO_4 under N_2 atmosphere (μC).

	GC	ZrO_{2-x}	Co_3O_{4-x}	TiO_{2-x}	SnO_{2-x}	Nb_2O_{5-x}
Oxidation	11.3	34.6	40.1	42.1	39.5	32.6
Reduction	11.8	35.4	42.4	42.0	39.7	32.7

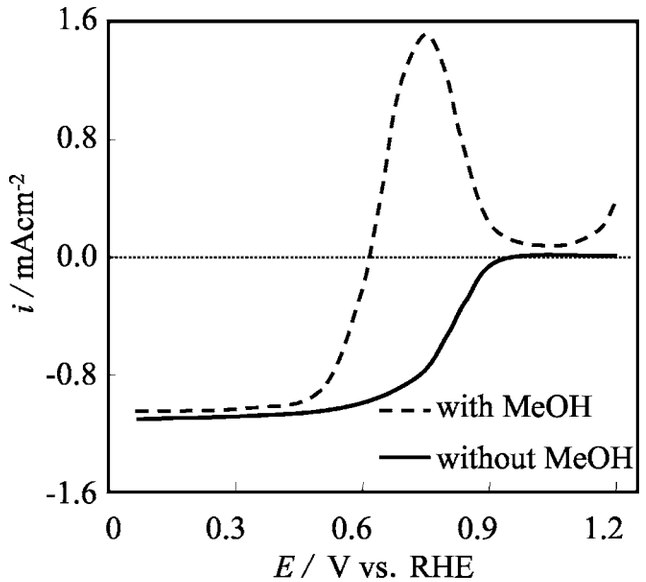

Figure 6. CVs in cathodic potential scan of the s-Pt under O_2 atmosphere 0.1 M H_2SO_4 without or with 0.1 M methanol.

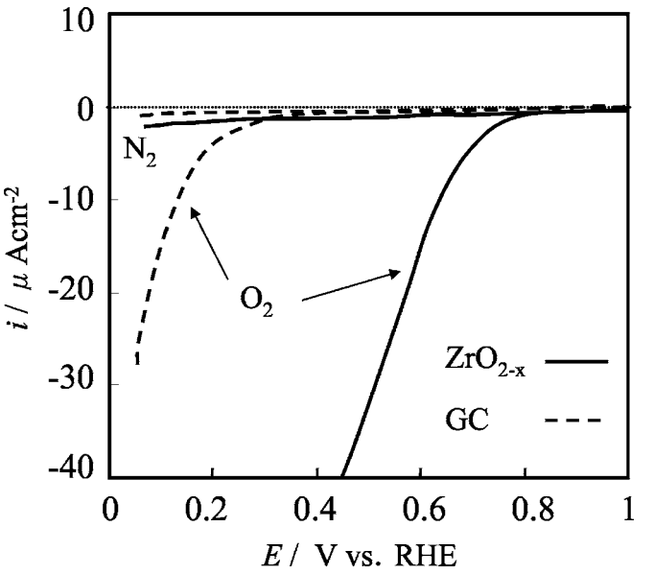

Figure 8. Potential-current curves of ZrO_{2-x} and GC under N_2 and O_2 atmosphere in 0.1 M H_2SO_4 with 0.1 M methanol at 30°C. Scan rate: 5 mV s^{-1}.

was scanned from 1.2 to 0.05 V with a scan rate of 5 mV s^{-1}. $E_{M-O}(-5)$ and $E_O(-5)$ express the potential at the reduction current density of -5 μA cm^{-2} with and without 0.1 M methanol, respectively. There was only a slight difference between the two curves in the presence and in the absence of methanol on all the sputtered metal oxides. The mixed potential as found on the Pt electrode was not observed on the metal oxide catalysts. This indicated that the oxygen reduction was not influenced by the presence of methanol. On the other hand, $E_O(-5)$ and $E_{M-O}(-5)$ of the s–Pt was 1.06 and 0.62 V, respectively. Compared to the potential in methanol-free electrolyte, a significant decrease of the potential was observed on the s–Pt electrode in the presence of methanol. It was obvious that the methanol effect on the oxygen reduction of the metal oxides was much less than that on the Pt. Moreover, $E_{M-O}(-5)$ of the ZrO_{2-x} was 0.68 V. It was 60 mV larger than that of the s-Pt.

As shown in Fig. 11, the potential ratio $R = E_{M-O}(-5)/E_O(-5)$ is defined as the evaluation indicator of the selectivity of the catalysts for the oxygen reduction in the presence of methanol. R of the s–Pt was 0.58, on the other hand, R of the metal oxides varied from 0.90 to 1.00. This reveals that the selectivity for the oxygen reduction on the metal oxides was higher than that of the Pt in the presence of methanol.

However, the ORR activity of these oxides still needs to be improved in comparison with the Pt. The relationship between the catalytic activity for the ORR and the physicochemical properties of

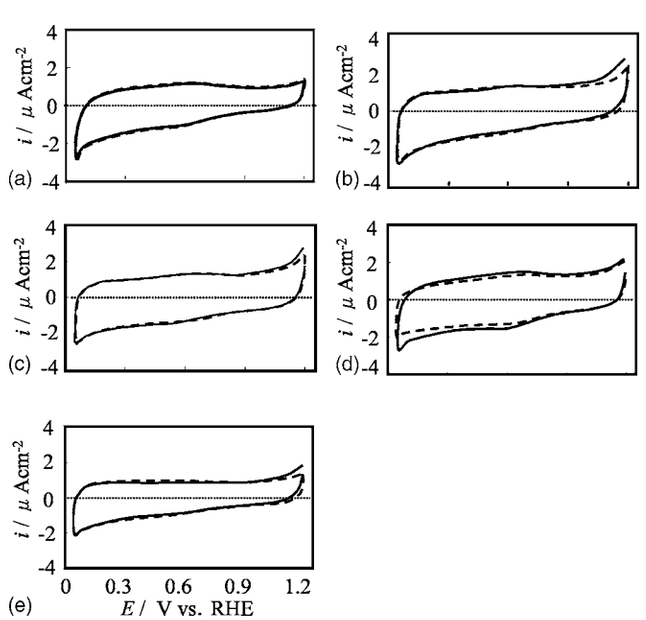

Figure 7. CVs of metal oxides under N_2 atmosphere in 0.1 M H_2SO_4 with or without 0.1 M methanol at 30°C. Scan rate: 5 mV s^{-1} with methanol (---), without methanol (—). (a) ZrO_{2-x}, (b) SnO_{2-x}, (c) TiO_{2-x}, (d) Co_3O_{4-x}, and (e) Nb_2O_{5-x}.

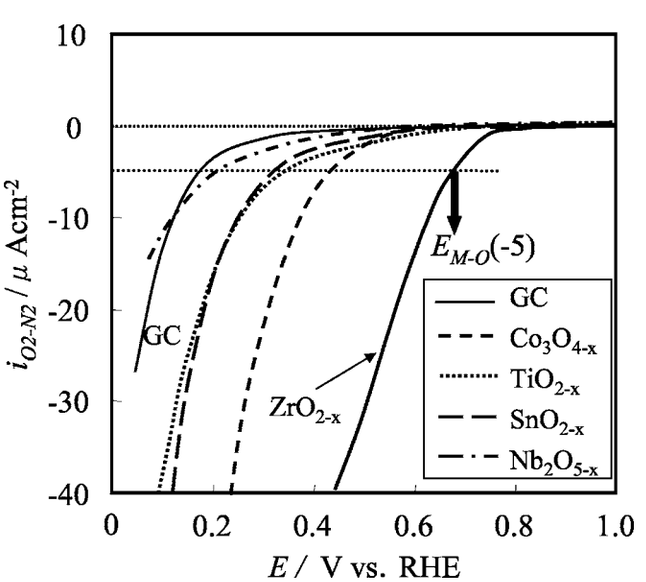

Figure 9. Potential-current curves of metal oxides under O_2 atmosphere in 0.1 M H_2SO_4 with 0.1 M methanol. Scan rate: 5 mV s^{-1}.

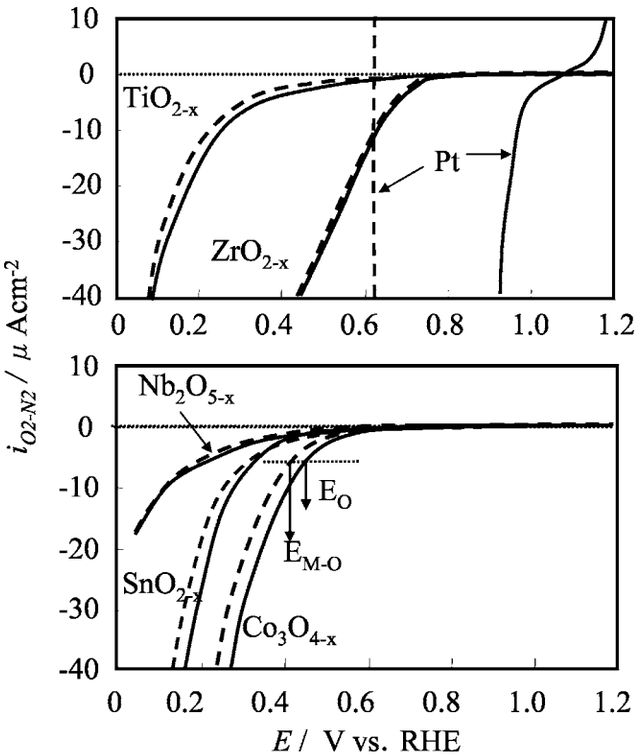

Figure 10. Potential-current curves of metal oxides under O_2 atmosphere in 0.1 M H_2SO_4 with or without 0.1 M methanol at 30°C. Scan rate: 5 mV s^{-1} with methanol (---), without methanol (—).

the oxides is very important and the key to improve the catalytic activity. The physicochemical properties and microstructure of the oxides controlled by the fabrication condition are under investigation. A detailed discussion will be reported in a future paper.

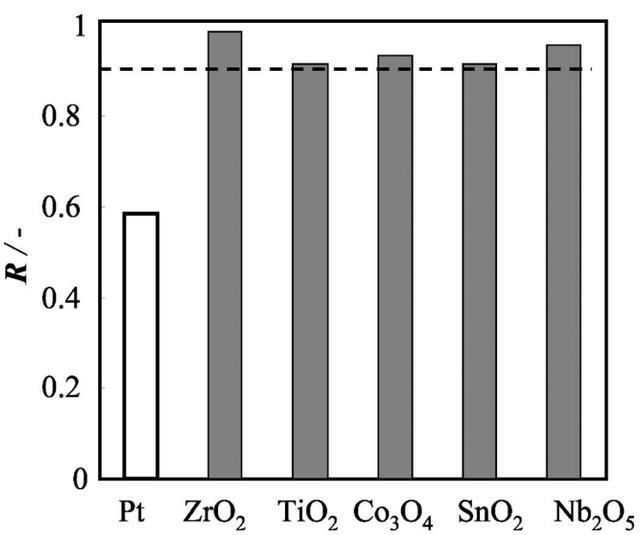

Figure 11. Potential ratio $R = E_{M\text{-}O}(-5)/E_O(-5)$ of metal oxides derived from Fig. 10.

Conclusions

Transition metal oxides (ZrO_2, TiO_2, SnO_2, Nb_2O_5, and Co_3O_4) were evaluated as new electrocatalysts for the cathode of DMFC. The catalytic activity for the oxygen reduction (ORR) of these transition metal oxides was evaluated in sulfuric acid with and without 0.1 M methanol. The sputtered metal oxides had stable states in acid medium at least in the potential range of the oxygen reduction. The metal oxides were not active for the methanol oxidation. The oxygen reduction activity of the metal oxides decreased in the following order: $ZrO_{2-x} > Co_3O_{4-x} > TiO_{2-x} \approx SnO_{2-x} > Nb_2O_{5-x}$ in the presence of methanol. Zirconium oxides showed the best activity for the oxygen reduction among these transition metal oxides. Moreover, in comparison with the potential at $i_{O_2-N_2} = -5$ μA cm^{-2}, ZrO_{2-x} was 60 mV larger than that of the s–Pt. This is due to the high selectivity of the metal oxides for the oxygen reduction. The mixed potential as found on the Pt electrode was not observed on the metal oxide catalysts. Zirconium oxides could be a good cathode substituting the platinum cathode for DMFCs.

Acknowledgments

The authors acknowledge the financial support received from the Japan Science and Technology Agency (JST) and the New Energy and Industrial and Technology Development Organization (NEDO).

Yokohama National University assisted in meeting the publication costs of this article.

References

1. M. K. Ravikumar and A. K. Shukla, *J. Electrochem. Soc.*, **143**, 2601 (1996).
2. J. T. Wang, S. Wasmus, and R. F. Savinell, *J. Electrochem. Soc.*, **143**, 1233 (1996).
3. A. Taniguchi, T. Akita, K. Yasuda, and Y. Miyazaki, Paper presented at the 71st Meeting of the Electrochemical Society of Japan (2004).
4. S. Mukerjee and S. Srinivasan, in *Handbook of Fuel Cells*, W. Vielstich, A. Lamm, and H. A. Gasteiger, Editors, p. 516, Wiley, New York (2003).
5. P. J. Ferreira, G. J. la O', Y. Shao-Horn, D. Morgan, R. Makharia, S. Kocha, and H. A. Gasteiger, *J. Electrochem. Soc.*, **152**, A2256 (2005).
6. P. Convert, C. Coutanceau, P. Crouïgneau, F. Gloagen, and C. Larmy, *J. Appl. Electrochem.*, **31**, 945 (2001).
7. R. Holze, I. Vogel, and W. Vielstich, *J. Electroanal. Chem. Interfacial Electrochem.*, **210**, 277 (1986).
8. B. Bittins-Cattaneo, S. Wasmus, B. A. Lopez de Mishima, and W. Vielstich, *J. Appl. Electrochem.*, **23**, 625 (1993).
9. R. Jiang and D. Chu, *J. Electrochem. Soc.*, **147**, 4605 (2000).
10. G. Lalande, R. Cotė, G. Tamizhmani, D. Guay, J. P. Dodelet, L. Dignard-Baley, L. T. Weng, and P. Bertrand, *Electrochim. Acta*, **40**, 635 (1995).
11. S. Gupta, D. Tryk, S. K. Zecevic, W. Aldred, D. Guo, and R. F. Savinell, *J. Appl. Electrochem.*, **28**, 673 (1998).
12. G. Q. Sun, J. T. Wang, S. Gupta, and R. F. Savinell, *J. Appl. Electrochem.*, **31**, 1025 (2001).
13. S. Gilman and D. Chu, in *Handbook of Fuel Cells*, W. Vielstich, A. Lamm, and H. A. Gasteiger, Editors, p. 659, Wiley, New York (2003).
14. N. Alonso-Vante, in *Proceeding of the 1st International Symposium of Fuel Cell Systems*, l'Ecole Polytechnique de Montrèal, p. 658 (1995).
15. N. Alonso Vante and H. Tributsch, *Nature (London)*, **323**, 431 (1986).
16. N. Alonso Vante, W. Jaegermann, H. Tributsch, W. Hönle, and K. Yvon, *J. Am. Chem. Soc.*, **109**, 3251 (1987).
17. C. Fischer, N. Alonso Vante, S. Fiechter, and H. Tributsch, *J. Appl. Electrochem.*, **24**, 1004 (1995).
18. O. Solorza-Feria, K. Ellmer, M. Giersig, and N. Alonso-Vante, *Electrochim. Acta*, **39**, 1647 (1994).
19. N. Alonso-Vante, H. Tributsch, and O. Solorza-Feria, *Electrochim. Acta*, **40**, 567 (1995).
20. N. Alonso-Vante, B. Schubert, and H. Tributsch, *Mater. Chem. Phys.*, **22**, 281 (1989).
21. Y. Liu, A. Ishihara, S. Mitsushima, N. Kamiya, and K. Ota, *Electrochem. Solid-State Lett.*, **8**, A400 (2005).
22. M. Pourbaix, *Atlas of Electrochemical Equilibria in Aqueous Solutions*, p. 324, Pergamon Press Ltd. New York (1966).
23. T. J. Schmidt, U. A. Paulus, H. A. Gasteiger, N. AlonsoVante, and R. J. Behm, *J. Electrochem. Soc.*, **147**, 2620 (2000).
24. D. Chu and S. Gilman, *J. Electrochem. Soc.*, **141**, 1770 (1994).
25. S. Gilman and D. Chu, in *Handbook of Fuel Cells*, W. Vielstich, A. Lamm, and H. A. Gasteiger, Editor, p. 655, Wiley New York (2003).